Nanotribological properties and mechanisms of alkylthiol and biphenyl thiol self-assembled monolayers studied by AFM

Bharat Bhushan* and Huiwen Liu
Computer Microtribology and Contamination Laboratory, 206 W. 18th Avenue, The Ohio State University, Columbus, Ohio 43210
(Received 25 September 2000; revised manuscript received 28 March 2001; published 5 June 2001)

Five kinds of alkylthiol and biphenyl thiol monolayers with different surface terminals, spacer chains, and head groups were prepared using a self-assembly method. The adhesion, friction, and wear properties were measured using atomic force microscopy (AFM). It is found that hexadecane thiol (HDT) with a-CH_3 terminal exhibits the smallest adhesive force and friction force because of the terminal group with its low work of adhesion and high-compliance long carbon chain. Experimental results and a meniscus analysis indicate that the adhesive force varies linearly with work of adhesion of self-assembled monolayers (SAMs). A molecular spring model is presented to clarify the lubrication mechanisms of SAMs. The molecular spring constant, as well as the inter molecular forces, dictates the magnitude of the coefficients of friction of SAMs. 4,4′-dihydroxybiphenyl (DHBp) on Si(111), due to its rigid biphenyl spacer chains, stronger interface bonds, and a hard substrate, has the best wear resistance. For all of the SAMs, the wear depth with normal load curves show critical normal loads. Below the critical normal load, SAMs undergo orientation, while at the critical normal load SAMs undergo severe wear at the interface due to the weak interfacial bond strengths. The influence of relative humidity on adhesive and frictional forces of SAMs can be mainly understood by comparing their terminal polarization properties and work of adhesion. At higher humidity, water capillary condensation can either increase friction through increased adhesion in the contact zone or reduce friction through an enhanced water-lubricating effect.

DOI: 10.1103/PhysRevB.63.245412 PACS number(s): 62.20.Qp, 68.37.Ps, 05.65.+b, 07.10.−h

I. INTRODUCTION

Microelectromechanical systems (MEMS) are expected to have a major impact on our lives, much like the way that the integrated circuit has affected information technology. MEMS industry revenue is approaching a billion dollars a year. Because of the large surface area to volume ratio in MEMS, the adhesive force and friction force dominate over inertial and gravitational forces. Recent studies have revealed the profound influence of stiction, friction, and wear on the efficiency, power output, and steady-state speed of microdynamic devices.[1,2] In fact, tribology of these devices appears to be a limiting technology. Reliability and the small size of MEMS necessitate the use of ultrathin lubricant films for protection of contacting surfaces.[3,4]

Langmuir-Blodgett (LB) and self-assembled monolayers (SAMs) techniques are the most common methods of forming monomolecular films on solid substrates for use as model lubricants.[5–8] However, in the case of LB films, the molecular interaction with the substrate through weak van der Waals forces, and repeated shearing results in rapid wear of the molecules. On the other hand, SAMs are ordered molecular assemblies formed by the chemical adsorption of an active surfactant on a solid surface and are therefore better candidates as lubricants. SAMs can be spontaneously formed by immersion of an appropriate substrate into a solution of an active surfactant in an organic solvent. This simple process makes SAMs inherently manufacturable and thus technologically interesting for building efficient lubricants.[5] SAMs consist of three building groups: a head group that binds strongly to a substrate, a tail group that constitutes the outer surface of the film, and a spacer chain (backbone chain) that connects the head and tail groups.[6,7] Because a large number of properties can be designed into SAMs, they offer almost unlimited possibilities for studies to correlate many surface and film parameters with friction and adhesion. For example, using molecules with different head groups, such as thiol (-SH), -silanes (-SiR_3), and acids (e.g. -COOH), can change the binding energy to the substrate. The elastic compliance can also be changed, for example, by modifying the chain length and/or the type of chemical bond inside the chains (single, double, and triple C-C bonds and benzene ring), by fluorination and/or by cross-linking. The tail groups that are exposed to the free surface of the film can also be conveniently tailored to control adhesion and friction.[5–7,9]

Early research by DePalma and Tillman,[10] Ando *et al.*,[11] and Ruhe *et al.*[12] indicated that self-assembled alkylsilane monolayers could be used as a lubricant on smooth silicon surfaces. However, tests in all these investigations were carried out using a traditional pin-on-disk tribotester under relatively large normal loads. Since they used high loads the relevance of these tests is questionable for MEMS. With the development of atomic force microscopy (AFM) techniques, researchers successfully characterized the nanotribological properties of self-assembled monolayers. Studies by Bhushan *et al.*[13] showed that C_{18} alkylsiloxane films exhibit the lowest coefficient of friction and can withstand much higher normal load during sliding as compared to LB films, soft Au films, and hard SiO_2 coatings. Liu *et al.*[14] observed the dependence of friction upon load and velocity. These early microtribological studies using AFM showed the possible utility of SAMs as lubricants in microdevices. Since then the micro- and nanotribological properties of SAMs have been studied using AFM by several groups.[5,9] The influence of chain length and surface terminal groups on frictional prop-

erties of SAMs has been mainly studied.[15–23]

To date only two types of self-assembled films have been widely studied: those derived from the adsorption and reaction of alkyltrichlorosilanes on the native oxide of silicon substrates and those formed from the adsorption of alkanethiols and disulfides on gold surfaces.[5,7,9,24] So far the nanotribological properties of SAMs, which have spacers consisting of benzene rings, have not been studied. The influence of head groups and cross-linking of spacer groups on the nanotribological performance of SAMs have also not been clearly studied. Besides these, the understanding of friction and wear mechanisms of SAMs, especially molecular level friction and wear mechanisms, is still lacking. The rapid development of the MEMS industry is stimulating the emerging needs of molecular design of SAMs for preparation of superior lubricants. The basis for molecular design and tailoring of SAMs must include a complete knowledge of interrelationships between the molecular structure and tribological properties of SAMs, as well as a deep understanding of the friction and wear mechanisms of SAMs at the molecular level.

For this purpose, five kinds of alkylthiol and biphenyl thiol SAMs with different surface terminals (-CH_3, -COOH, and -OH) and head groups (-SH and -OH) were prepared. Hexadecane thiol (HDT), 16-mercaptohexadecanoic acid thiol (MHA), 1, 1′-biphenyl-4-thiol (BPT) and cross-linked BPT (BPTC) were deposited on Au(111) substrates. A 4, 4′-dihydroxybiphenyl (DHBp) film was deposited on a hydrogenated Si(111) substrate. The influences of spacer chains (carbon chain and biphenyl chain), crosslinking of biphenyl spacers and the head groups (-SH and -OH) on the nanotribological properties of SAMs were investigated by AFM. The adhesion, friction, and wear mechanisms of SAMs at the molecular scale are discussed. A molecular spring model is presented to clarify the frictional behavior of SAMs.

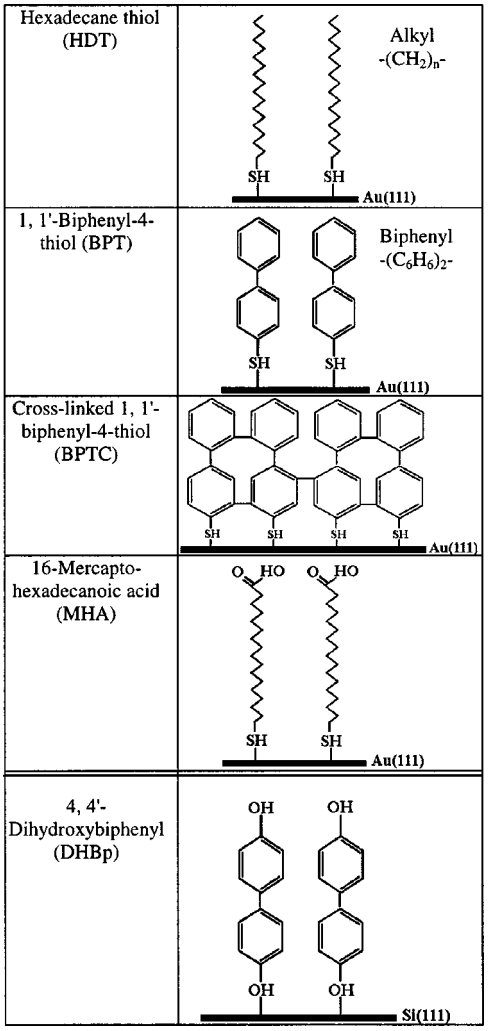

FIG. 1. Schematics of the structures of HDT, BPT, MHA, DHBp, and BPTC SAMs.

II. EXPERIMENTAL DETAILS

A. Preparation of SAMs

HDT, MHA, and DHBp were purchased from Aldrich and used as received. BPT was synthesized by thermal rearrangement of 1, 1′-biphenyl-4-O-(*N*,*N*-dimethyl)-thiocarbamate in bulk at 230 °C. 30-nm Au(111) films were prepared by thermal evaporation on a Si(111) substrate. Before SAM preparation, the gold surface was cleaned by 10 min of UV irradiation in air (254 nm, 150 W, 3 cm distance). The glassware for preparation of various solutions and for the self-assembly was cleaned with the ''piranha'' solution (mixture of 3:1 v/v of H_2SO_4 and 30% H_2O_2) at 80 °C.

HDT and MHA monolayers were prepared by 24 h immersion of the Au(111)/Si(111) substrates in 1 mmol HDT and MHA solutions in ethanol, respectively. The BPT monolayer was formed by immersion of Au(111)/Si(111) substrates for 72 h in a degassed solution of 15 mmol BPT in *N*,*N*-dimethylformamide under nitrogen. The DHBp monolayer was prepared by treating hydrogenated Si(111) wafers with a 1% solution of DHBp in anhydrous anisole at 100 °C for 16 h in a nitrogen atmosphere. The cross-linked 1, 1′-biphenyl-4-thiol monolayer (BPTC) was generated by irradiation of BPT monolayers with 50-eV electrons. IR spectra indicated that stretching vibration peaks of the aromatic C-H groups and the semicircle stretch and breathing mode peaks of the phenyl ring decrease significantly after exposure to 3000 $\mu C/cm^2$ and completely disappear after exposure to 10 000-$\mu C/cm^2$ electrons. This indicates the formation of cross-links between neighboring biphenyls by electron-induced cleavage of C–H bonds.[25]

Figure 1 schematically shows the structures of the five kinds of SAMs prepared in this study. It shows that HDT and MHA have the same heads and spacers, but different terminals; their surface terminals are $-CH_3$ and -COOH, respectively. BPT and DHBp have the same spacers, but the head and tail groups of DHBp are -OH instead of -SH and -CH in BPT. Figure 1 also shows that when compared with BPT, there are cross-linking bonds between neighboring biphenyls in BPTC.

B. Advancing-contact-angle measurement

The advancing contact angle was measured using a Rame-Hart model 100 contact-angle goniometer. Distilled water

was applied on the sample surfaces using a fine injector. Two measurements of the contact angle at 22 °C and 45–55 % relative humidity (RH) were performed on opposite edges of at least three droplets. The contact angles were typically reproducible to within ±2°. The variation of the advancing contact angle with rest time was carried out during 7 min of the formation of the water droplet.

C. AFM measurements

Adheison and friction tests were carried out with a commercial AFM system (Nanoscope III, Digital Instrument) operating under ambient conditions of 22 °C and 45–55 % RH. Square pyramidal Si_3N_4 tips with a nominal 30–50-nm radius mounted on gold-coated triangular Si_3N_4 cantilevers with spring constants of 0.58 N/m were used. Surface roughness and friction images were obtained simultaneously, and the local relationship between the two images could be established. All scanning was performed in a direction perpendicular to the long axis of the cantilever beam. Adhesive force measurements were performed in the force calibration mode. By measuring the friction force as a function of normal load, an average value of the coefficient of friction was obtained. The friction force was calibrated by the method described in Refs. 2 and 26. For each sample the friction and adhesive forces were measured at at least six different locations.

A single-crystal natural diamond tip was used for wear tests.[13] The diamond tip is ground to the shape of a three-sided pyramid with an apex angle of 80° and a tip radius of about 100 nm. The tip is bonded with epoxy to a gold-coated, 304 stainless steel, rectangular cantilever beam (thickness = 20 μm, width = 0.2 mm, and length = 20 mm). The stiffness of the beam is obtained by approximating it to be the spring constant of an end-loaded cantilever beam of rectangular cross section, which is given by

$$K = Et^3w/4l^3, \tag{1}$$

where E is the elastic modulus, t is the thickness, w is the width, and l is the length of the cantilever beam. By changing the length of the beam in the cantilever holder, the desired spring constant can be obtained. In this study, typical normal loads used for the wear studies ranged from 0.5 to 31 μN with a cantilever stiffness of about 14.9 N/m. Periodically, the tip was scanned on a clean single-crystal silicon sample to find out whether the tip was contaminated. If the adhesive force measurement indicated any contamination, then the tip was carefully cleaned with an alcohol-soaked cotton swab under an optical microscope. For comparison, all AFM data presented in the same plot were obtained with a single cantilever.

Tests of the influence of relative humidity on the adhesive and frictional forces were performed in an environmentally controlled chamber. The relative humidity ranged from 0% to 60%. In each test, the sample and tip were kept in the environment for at least two hours to allow let the system to reach equilibrium.

III. RESULTS AND DISCUSSION

A. Roughness of SAMs

Surface height and friction force images were recorded simultaneously over a region of 1 μm × 1 μm. Figure 2 shows gray-scale images of surface height and friction force. The topography of Au(111) film and SAMs deposited on Au(111) substrates appear to be granular. For Au(111), HDT, MHA, and BPTC, a good correlation between the surface height and the corresponding friction force images was observed. It was noticed that the friction force changed with surface height in the same direction (upwards and downwards) in both trace and retrace friction profiles of the friction loop. Thus the change in friction force corresponds to transitions in surface slope.[27,28] Figure 2 also indicates that the topography and friction images of Si(111) and DHBp/Si(111) are very similar; they exhibit featureless surfaces and their friction force images do not show any abrupt changes.

For further analysis presented later in this work, the roughness, thickness, tilt angles, and spacer chain lengths of Si(111), Au(111), and various SAMs are listed in Table I. The thickness, tilt angles, and spacer chain length are cited from the literature.[7,25,29,30] The roughness of BPT and MHA are very close to that of Au(111). But the roughness of BPTC is lower than that of Au(111) and BPT, this is caused by electron irradiation. Table I indicates that the roughness values of HDT and DHBp are much higher than their substrate roughness of Au(111) and Si(111), respectively. This is caused by local aggregation of organic compounds on the substrates during SAMs deposition. Table I also indicates that the thickness of biphenyl thiol SAMs are generally thinner than the alkylthiol thickness, which is responsible for the shorter spacer chain in biphenyl thiol.

B. Adhesion, contact angle, and work of adhesion

The average values and standard deviation of the adhesive force measured by the force calibration method are presented in Fig. 3. It shows that SAMs can reduce the adhesive force of Si(111) and Au(111). In particular, the use of HDT and BPTC can significantly reduce the adhesive force of Si(111) and Au(111). Based on the data, the ranking of adhesive forces F_a is in the following order: $F_{a\text{-Au}}(48.0\,\text{nN}) > F_{a\text{-Si}}(43.7\ \text{nN}) > F_{a\text{-DHBp}}(36.5\ \text{nN}) \approx F_{a\text{-MHA}}(36.0\ \text{nN}) > F_{a\text{-BPT}}(28.7\,\text{nN}) > F_{a\text{-BPTC}}(20.8\,\text{nN}) > F_{a\text{-HDT}}(14.0\,\text{nN})$.

In micro- and nanoscale contact, water capillary condensation is believed to influence the adhesive and frictional forces. In the case of a sphere in contact with a flat surface, the attractive Laplace force caused by water capillary is

$$F_L = 2\pi R\gamma_{la}(\cos\theta_1 + \cos\theta_2), \tag{2}$$

where R is the radius of the sphere, γ_{la} is the surface tension of the liquid against air, and θ_1 and θ_2 are the contact angles between liquid and flat and spherical surfaces, respectively.[4] In our AFM adhesive study, the tip–flat-sample contact is just like a sphere in contact with a flat surface, and the liquid is water. Since a single tip was used in the adhesion measurements, we can treat $\cos\theta_2$ as a constant. So we can write

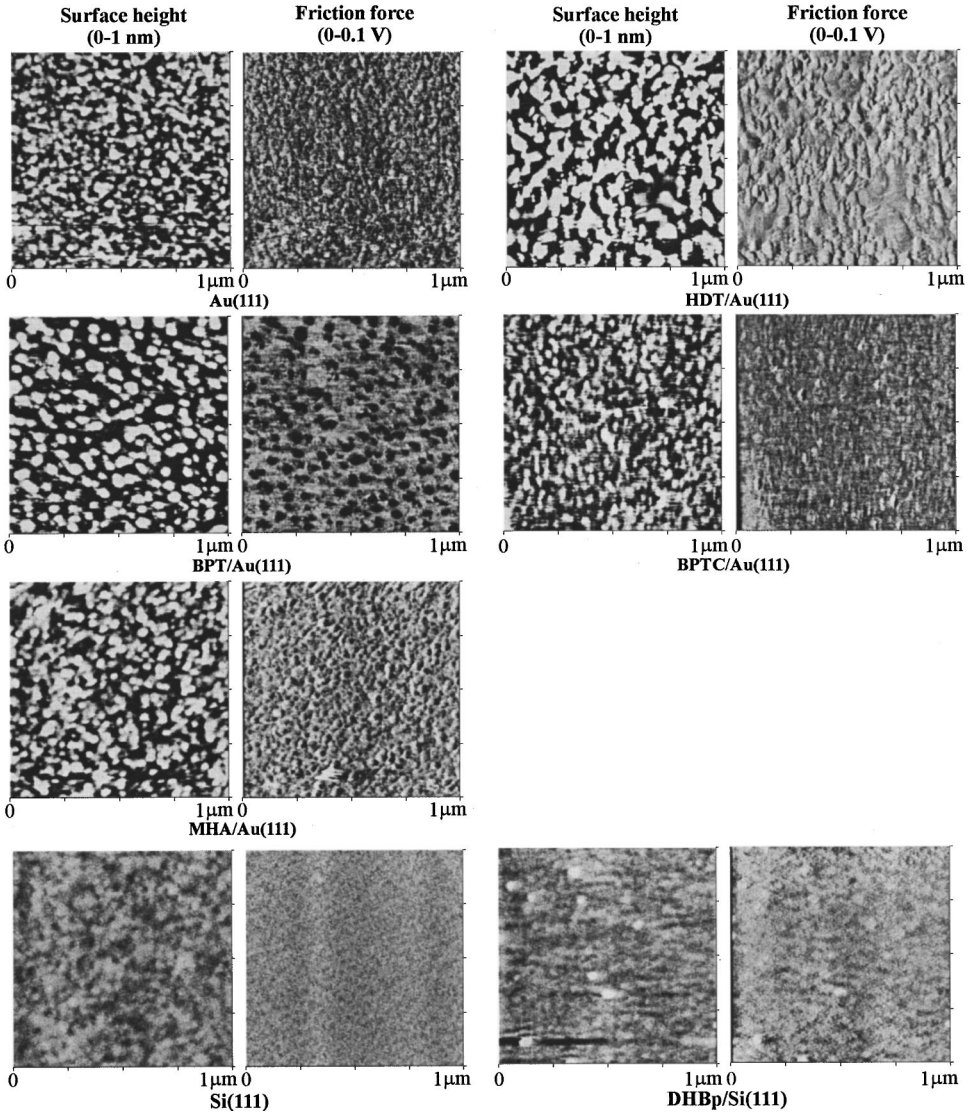

FIG. 2. Atomic force microscopy gray-scale height and friction force images of Si(111), Au(111), HDT, BPT, MHA, DHBp, and BPTC. The scan size was 1 μm$\times$1 μm, and the normal load was 3.3 nN.

$$F_L = 2\pi R\gamma_{la}(1+\cos\theta_1) - 2\pi R\gamma_{la}(1-\cos\theta_2)$$

$$= 2\pi R\gamma_{la}(1+\cos\theta_1) - C, \tag{3}$$

where C is a constant.

Based on the following Young-Dupre equation, work of adhesion W_a (the work required to pull apart the unit area of the solid-liquid interface) can be written as[31]

$$W_a = \gamma_{la}(1+\cos\theta_1). \tag{4}$$

It indicates that W_a is determined by the contact angle of SAMs, i.e., is influenced by the surface chemistry properties of SAMs. By substituting Eq. (4) into Eq. (3), F_L can be expressed as

$$F_L = 2\pi R W_a - C. \tag{5}$$

When the influence of other factors, such as the van der Waals force, are very small on the adhesive force, then the adhesive force $F_a \approx F_L$. Thus the adhesive force F_a should be proportional to work of adhesion W_a.

TABLE I. The R_a roughness, thickness, tilt angles and spacer chain lengths of SAMs.

Samples	R_a roughness[a] (nm)	Thickness[b] (nm)	Tilt angle[b] (deg)	Spacer length[c] (nm)
Si(111)	0.07			
Au(111)	0.37			
HDT	0.92	1.89	30	1.91
BPT	0.36	1.25	15	0.89
BPTC	0.14	1.14	25	0.89
MHA	0.37	2.01	30	1.91
DHBp	0.25	1.13		0.89

[a]Measured by an AFM with 1 μm$\times$1 μm scan size, using a Si_3N_4 tip under a 3.3-nN normal load.

[b]The thickness and tilt angles of BPT, BPTC, and DHBp are cited from Ref. 25. The thickness and tilt angles of HDT and MHA are cited from Ref. 7.

[c]The spacer chain lengths of alkylthiols were calculated by the method in Ref. 29. The spacer chain lengths of biphenyl thiols were calculated based on the data in Ref. 30.

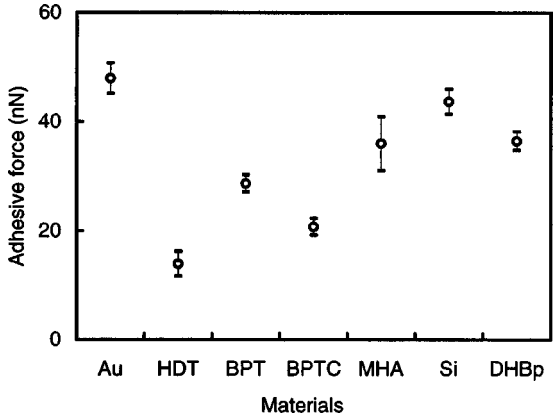

FIG. 3. Adhesive forces of Si(111), Au(111), and SAMs measured using force calibration method. For each sample, the adhesive forces were measured at least six times at different locations on the surface.

The contact angles of distilled water on Si(111), Au(111), and SAMs were measured using a contact-angle goniometer. After dropping water on the sample surfaces, the dynamic advancing contact angle (DACA) was measured with a frequency of 60 s for spontaneous spreading for at least 420 s. The DACA as a function of time data is given in Fig. 4(a). It indicates that there is a linear relationship between the DACA and rest time. As defined by many authors, the static advancing contact angle (SACA) (at $t=0$) should be used for surface characterization.[32–34] This SACA can be obtained by simple extrapolation of the data in Fig. 4(a) to $t=0$. The SACA of Si(111), Au(111), and SAMs is summarized in Fig. 4(b). For water, $\gamma_{la}=72.6\,\mathrm{mJ/m^2}$, using Eq. (4), the work of adhesion data are presented in Fig. 4(c). Based on Fig. 4(c), the work of adhesion W_a can be ranked in the following order: $W_{a\text{-Si}}(117.0) > W_{a\text{-DHBp}}(98.8\,\mathrm{mJ/m^2}) \approx W_{a\text{-MHA}}(101.8\,\mathrm{mJ/m^2}) \approx W_{a\text{-Au}}(97.1\,\mathrm{mJ/m^2}) > W_{a\text{-BPT}} \times (86.8\,\mathrm{mJ/m^2}) > W_{a\text{-BPTC}}(82.1\,\mathrm{mJ/m^2}) > W_{a\text{-HDT}} \times (61.4\,\mathrm{mJ/m^2})$. Except $W_{a\text{-Au}}$, this order exactly matches the order of F_a in Fig. 3. The relationship between F_a and W_a is summarized in Fig. 5. It indicates that the adhesive force F_a (nN) increases with work of adhesion W_a ($\mathrm{mJ/m^2}$) by the following linear relationship:

$$F_a = 0.57 W_a - 22. \tag{6}$$

These experimental results agree well with the modeling prediction presented earlier in Eq. (5). It proves that in this study the adhesive forces of SAMs are mainly influenced by the capillary force. The reason that Au shows higher adhesive force is still not completely clear. But easy attachment of Au on the tip should be one of the reasons.

C. Frictional properties of SAMs

Figure 6 shows some representative results of friction versus normal load curves for SAMs. Each curve was obtained by making measurements at increasing loads. The nonzero value of the friction signal at zero external load is due to the adhesive forces that cause the jump-to-contact instability during approach of the tip to the sample surface. As seen in

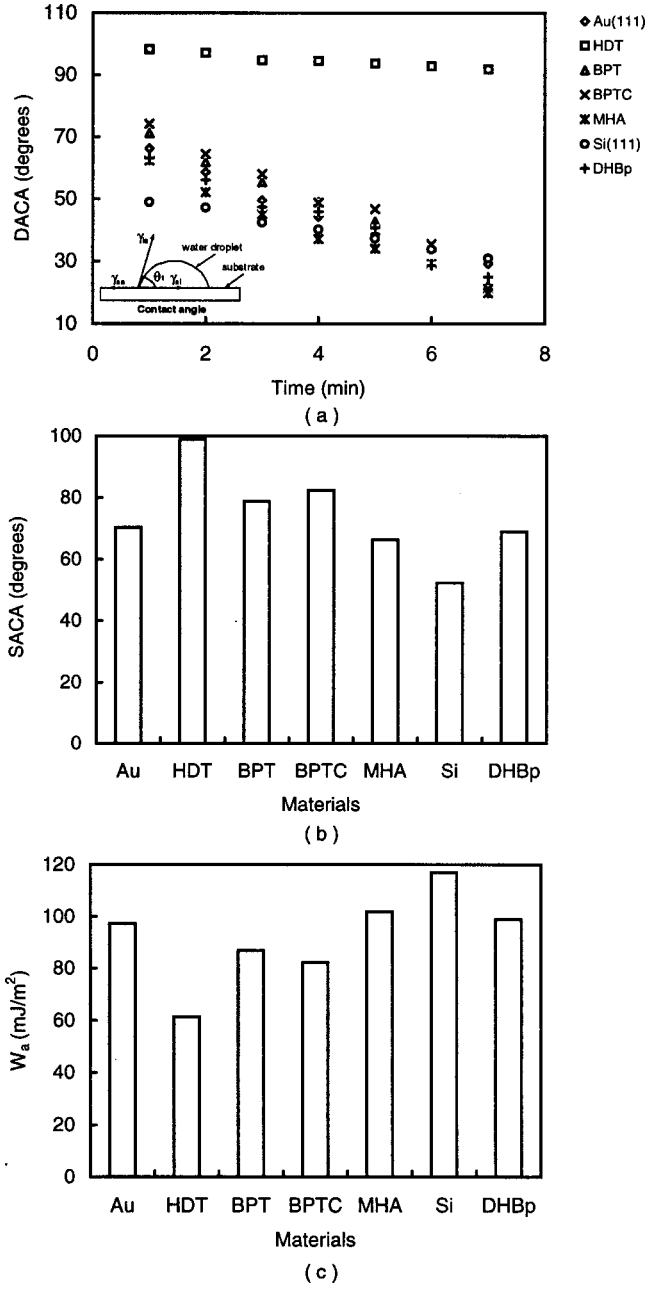

FIG. 4. (a) Variation of dynamic advancing contact angle (DACA) with time. All of the points in this figure represent the mean value of six measurements. The uncertainty associated with the average friction is within $\pm 2°$. (b) The static advancing contact angle (SACA) of Si(111), Au(111), and SAMs. (c) work of adhesion of Si(111), Au(111), and SAMs. The insert schematic in Fig. 4(a) shows the contact angle of the water droplet on the sample surface.

Fig. 6, an approximately linear response is observed, which suggests that no substantial plastic deformation occur in the testing range. The frictional forces of SAMs are consistently smaller than that for Si(111). The coefficient of friction values and their standard deviation are summarized in Fig. 7. It shows that alkylthiol and biphenyl thiol SAMs can be used as effective molecular lubricants for silicon, and HDT exhibits the smallest coefficient of friction.

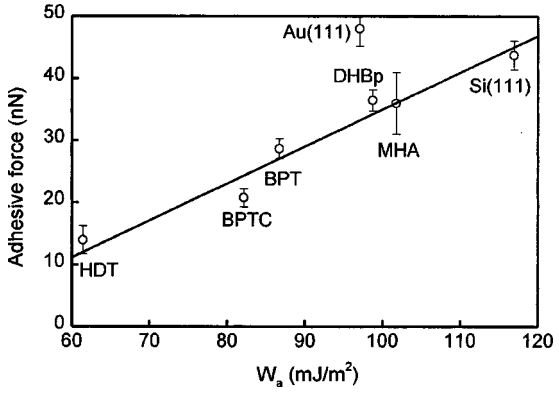

FIG. 5. The relationship between the adhesive forces and work of the adhesion.

Next we examine the friction mechanisms of SAMs. Monte Carlo simulation of the mechanical relaxation of $CH_3(CH_2)_{15}SH$ self-assembled monolayer performed by Siepmann and McDonald[35] indicated that SAMs respond nearly elastically to microindentation of an AFM tip under a critical normal load. They also suggested that under the given conditions, the monolayer could be compressed to 25% of its initial thickness. Compression also leads to major changes in the mean molecular tilt and in the distribution of conformational defects along the chains, but the original structure is recovered as the load is removed. Recent AFM studies of SAMs proved these predications derived by Monte Carlo simulation.[36,37] Garcia-Parajo *et al.*[36] observed the effect of compression while the load is being applied to an octadecyltrichlorosilane (OTS) film. Lio *et al.*[37] observed that *n*-alkanethiols become disordered at higher load. Thus we suggest that the chemical adsorbed self-assembled molecules on a substrate are just like assembled molecular springs anchored to the substrates. In order to explain the frictional difference of SAMs, a molecular spring model is presented in Fig. 8. It is assumed that a Si_3N_4 tip sliding on the surface of SAMs is like a tip sliding on the top of ''molecular springs or brush.'' The molecular spring assembly has compliant features and can experience orientation and

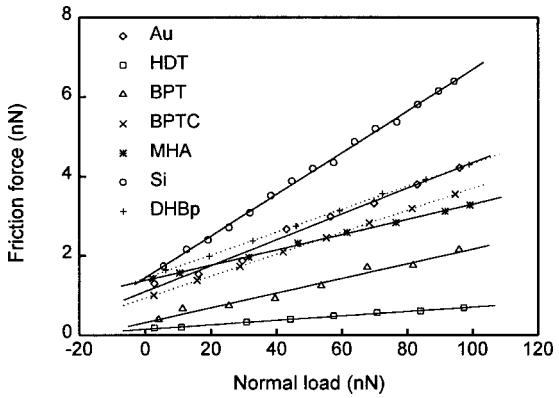

FIG. 6. Friction as a function of normal load curves obtained for Si(111), Au(111), and SAMs. All of the points in this figure represent the mean value of six measurements. The uncertainty associated with the average friction is within $\pm 7\%$.

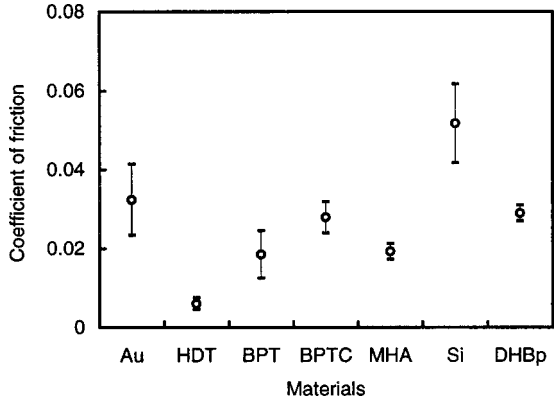

FIG. 7. Coefficient of friction for Si(111), Au(111), and SAMs measured using the force calibration method. For each sample, the adhesive forces were measured at least six times at different locations on the surface.

compression under normal load. The orientation of the ''molecular springs or brush'' under normal load reduces the shearing force at the interface, which in turn reduces the friction force. The possibility of orientation is determined by the spring constant of a single molecule, as well as the interaction between the neighboring molecules, which can be reflected by packing density or packing energy. It was estimated by Lio *et al.*[37] that the spring constant of a single alkanethiol molecule would be 3 N/m (for the assumed value of $E=36$ GPa) based on the simulation of Siepmann and McDonald.[35] So far it is difficult to calculate the spring constant of biphenyl thiol using their model, since the model of Siepmann and McDonald is based on alkylthiol. However, from the view of molecular structures, biphenyl thiol is a

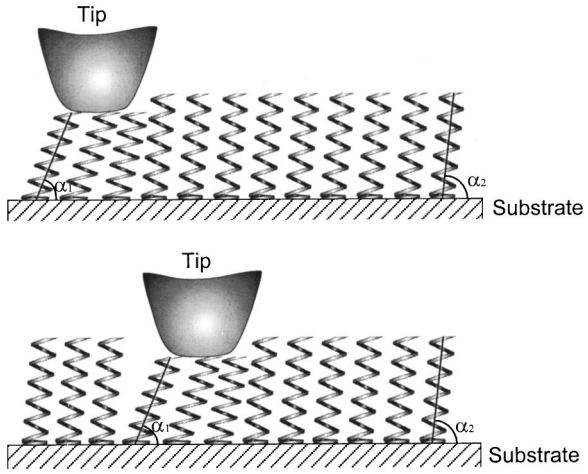

FIG. 8. Molecular spring model of SAMs. In this figure, $\alpha_1 < \alpha_2$, which is caused by the orientation under the normal load applied by the AFM tip. The orientation of the molecular springs reduces the shearing force at the interface, which in turn reduces the friction force. In elasticity deformation range, when the tip slips away, the orientated and compressed molecules can recover to their initial state. The molecular spring constant, as well as the intermolecular forces can determine the magnitude of the coefficients of friction SAMs. In this figure, the size of the tip and molecular springs are not in exactly the same scale.

more rigid structure due to the contribution by two benzene rings. Therefore the spring constant of BPT should be larger than that of HDT. The hydrogen (H^+) in a biphenyl chain has a strong static electron attractive force with the π electrons in the neighboring benzene ring. Thus the intermolecular force between biphenyl chains is stronger than that for alknethiol chains. The larger spring constant of BPT and stronger intermolecular force require a larger external force to allow it to orient, thus causing higher coefficient of friction. For MHA and DHBp, their basic chain structures are very close to HDT and BPT, but their surface terminals are different. The polar -COOH and -OH external functional groups in MHA and DHBp increase the adhesive force, which in turn increases the normal force, thus leading to higher friction force. The cross-linking of BPT leads to a larger packing energy for BPTC. Therefore it requires a larger external force to allow BPTC orientation, i.e., the coefficient of BPTC is higher than that in BPT.

In summary, we found that HDT exhibits the smallest coefficient of friction. SAMs exhibit compliance and can experience orientation under normal load. The orientation of SAMs reduces the shear stress at the interface; therefore SAMs can serve as good lubricants. The molecular spring constant, as well as the intermolecular forces can influence the magnitude of the coefficients of friction of SAMs.

D. Wear properties of SAMs

Wear resistance was studied using a diamond tip on an area of 1 μm$\times$1 μm. The variation of wear depth with normal loads is presented in Fig. 9. The section profiles of the wear scars under a 6.5-nN normal load are presented in Fig. 10. Figures 9 and 10 clearly show that in the whole testing range, DHBp on Si(111) exhibits much better wear resistance compared to Si(111), Au(111), and other SAMs that were deposited on the Au(111) substrate. For the SAMs deposited on Au(111), HDT has the best wear resistance. For all of the tested SAMs, in the wear depth versus normal load curves, there appears a critical normal load that is marked by arrows in Fig. 9. When the normal loads are smaller than the critical normal loads, the monolayers only show slight height changes in the scan areas. When the normal loads are higher than the critical values, the wear depths of SAMs increase dramatically.

Barrena *et al.*[38] observed that the height of self-assembled alkylsilanes decrease in discrete amounts with normal load. This steplike behavior is due to the discrete molecular tilts, which are dictated by the geometrical requirements of the close packing of molecules. Only certain angles are allowed due to the zigzag arrangement of the carbon atoms. The relative height of the monolayer under pressure can be calculated by the following equation:

$$\frac{h}{L}=\left[1+\left(\frac{na}{d}\right)^2\right]^{1/2}, \tag{7}$$

where L is the total length of the molecule in the all-trans configuration, h is the height of the SAMs in the tilt configuration (monolayer thickness), a is the distance between alternate carbon atoms in the molecule, d is the separation of the

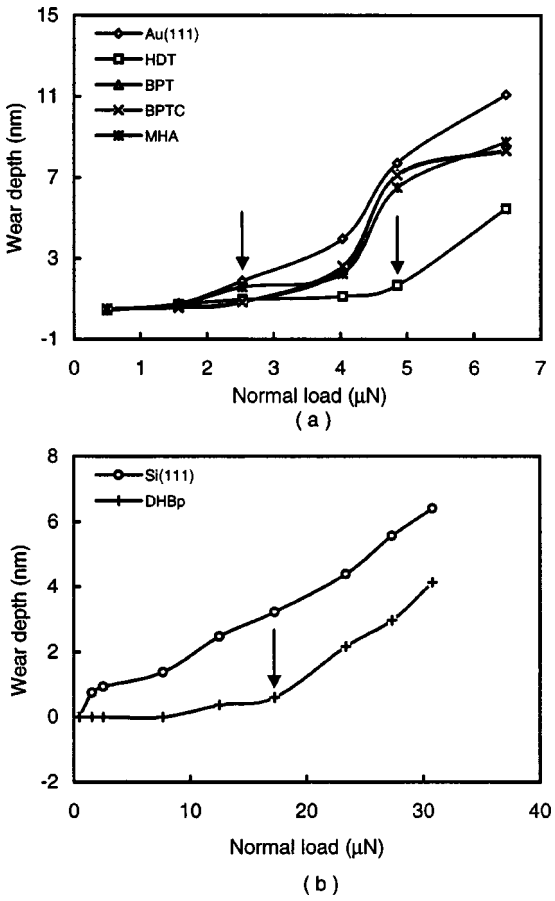

FIG. 9. Wear depth as a function of normal load after one scan cycle. All of the data points in this figure are the average value of three measurements.

molecules, and n is the step number. For HDT and MHA, only the head groups are different in their work and our work. The spacer carbon chains in alkanethiol and alkylsilane are exactly the same. So we use the same a (0.25 nm) and d (0.47 nm) values in our calculation for HDT and MHA. The calculated and measured relative heights of HDT and MHA are listed in Table II. When the normal loads are smaller than the critical values, the measured relative height values of HDT and MHA are very close to the calculated values. It means that HDT and MHA underwent step tilting below critical normal loads. Since we do not know the d value for biphenyl thiols, we cannot perform the above calculation for BPT, BPTC, and DHBp. However, their wear behavior under critical loads is very similar to alkanethiol SAMs. Therefore, it is reasonable to infer that they may also undergo orientation below critical loads.

The residual SAM thickness after wear under critical normal load was measured by profiling the worn film using AFM. The results are listed in Table III. For an alkanethiol monolayer, the relationship between the monolayer thickness h and intercept length L_0 can be expressed as (see Fig. 11)

$$h=b\cos(\alpha)n+L_0, \tag{8}$$

where b is the length of the projection of the C–C bond onto the main chain axis ($b=0.127$ nm for alkanethiol), n is the

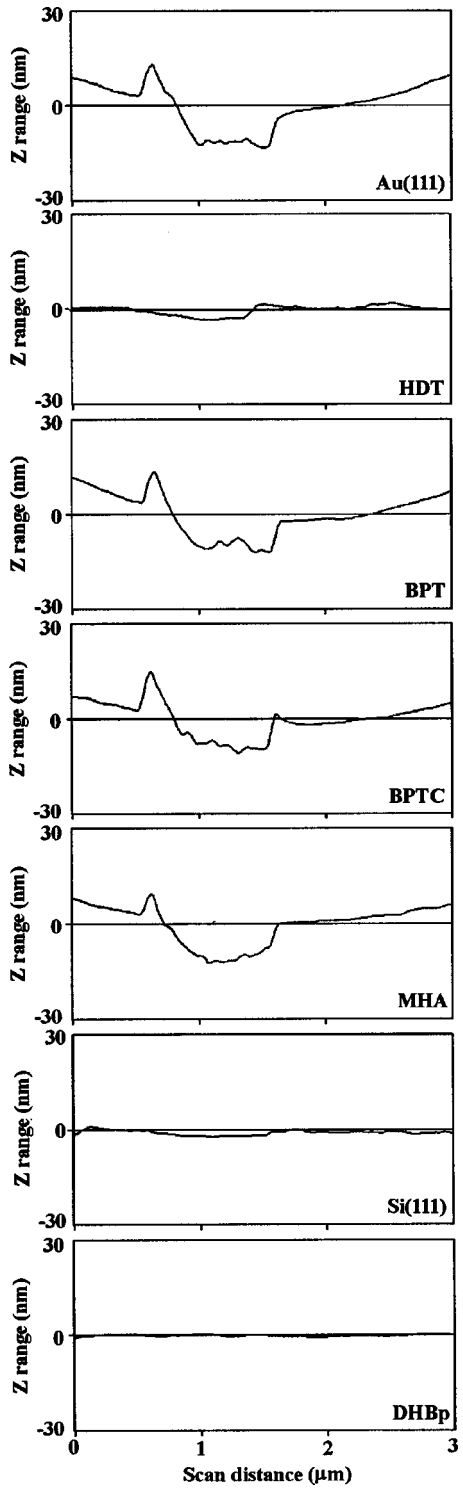

FIG. 10. The section profiles of Si(111), Au(111), and SAMs under a 6.5-μN normal load.

chain length defined by $CH_3(CH_2)_nSH$, and α is the tilt angle.[29] For BPT and BPTC, based on the same principle, and using the bond lengths reported in Ref. 30, the L_0 values are also calculated. The calculated L_0 and measured residual film thickness for SAMs under critical load are summarized in Table III. Table III indicates that the measured residual thickness values of SAMs under critical load are very close to the calculated intercept length L_0 values. It means that under the critical normal load, the Si_3N_4 tip approaches the interface and SAMs wear severely away from the substrate. This is due to the interface chemical adsorption bond strength (HS-Au and Si-O) being generally smaller than the other chemical bond strengths in SAMs (see Table IV). Based on these discussion, it is believed that the reason why DHBp has the best wear resistance is due to the rigid biphenyl rings structure (compared to carbon chain in alkylthiol), the hard Si(111) substrate [compared to Au(111) substrate], and the strong interface Si-O bond strength (compared to the weak HS-Au bond strength in the other SAMs, see Table IV).

In summary, in all SAMs DHBp has the best wear resistance. The variation of wear depths with normal load exhibits critical normal loads. Below the critical normal load, SAMs undergo orientation, while at the critical normal load SAMs undergo severe wear at the interface due to the weak interface bond strengths. In order to improve wear resistance, the interface bond must be enhanced; rigid spacer chains and a hard substrate are also preferred.

TABLE II. Calculated $[1+(na/d)^2]^{1/2}$ and measured (h/L) relative heights of HDT and MHA self-assembled monolayers.

Steps n	Calculated[a] $[1+(na/d)^2]^{1/2}$	Measured[b] HDT	Measured[b] MHA
1	0.883		
2	0.685	0.674[c]	0.643[c]
3	0.531	0.532[d]	0.552[d]
4	0.425	0.416[e]	
5	0.352	0.354[f]	
6	0.299		

[a]Calculations are based on the assumption that the molecules tilt in discrete steps (n), upon compression with a diamond AFM tip (Ref. 38).
[b]Measured values are the mean value of three tests.
[c]Normal load of 0.5 μN.
[d]Normal load of 1.57 μN.
[e]Normal load of 2.53 μN.
[f]Normal load of 4.03 μN.

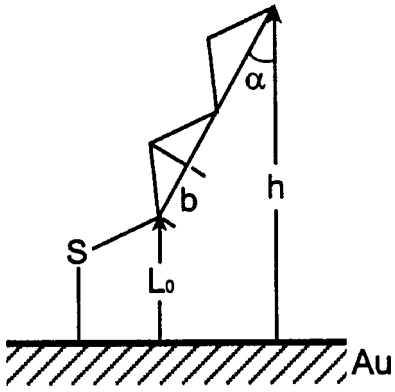

FIG. 11. Illustration of the relationship between the components of the equation $h=b\cos(\alpha)n+L_0$.

TABLE III. Calculated L_0 and measured residual film thickness for SAMs under critical load.

	L_0 (nm)[a]	Residual thickness[b] (nm)
		0.25
HDT	0.24	0.42
BPT	0.39	0.38
BPTC	0.33	0.29
MHA	0.36	
DHBp		0.52

[a]Calculated by the equation of $h=b\cos(\alpha)n+L_0$ (Ref. 29).
[b]Measured by AFM using a diamond tip under critical normal load. All of the data are the mean value of three tests.

E. Influence of relative humidity on adhesion and friction

The influence of relative humidity on adhesion and friction was studied in an environmentally controlled chamber. The results are presented in Fig. 12. Figure 12 shows that for Si(111), Au(111), DHBp, and MHA, the adhesive and frictional forces increase with relative humidity. For BPT and BPTC, the adhesive force only slightly increases with relative humidity when the relative humidity is higher than 40%, but it is very interesting that their coefficients of friction decrease slightly in the same range. For HDT, in the testing range, the adhesive and friction forces are not sensitive to changes in relative humidity.

The possibility of forming a water capillary is related to surface terminal polarization properties. The polar groups are easily anchored to water molecules to form a water capillary. We already have shown that the adhesive force is linearly related to the work of adhesion of the surfaces. Si(111), DHBp, and MHA have polar surface terminals and larger works of adhesion. Therefore this must lead to the larger adhesive forces in higher relative humidity. The larger intrinsic adhesive force will add to the normal load, which in turn increases the friction force for these samples. In contrast, HDT has a nonpolar-CH_3 surface terminal and a very small work of adhesion; thus the adhesive force and friction force of HDT are not sensitive to the change of humidity. The work of adhesion of BPT and BPTC is between that of Si(111) and HDT (see Fig. 5); therefore their adhesive forces show a slight increase when RH$>$40%. The fact that BPT and BPTC show a lower friction force when RH$>$40% indicates that a thin adsorbed water layer can act as a lubricant.

The influence of relative humidity on adhesive and frictional forces can be primarily understood by comparing their surface terminal polarization properties and work of adhesion. At higher humidity, water capillary condensation can either increase friction through increased adhesion in the contact zone or reduce friction through an enhanced water-lubricating effect.

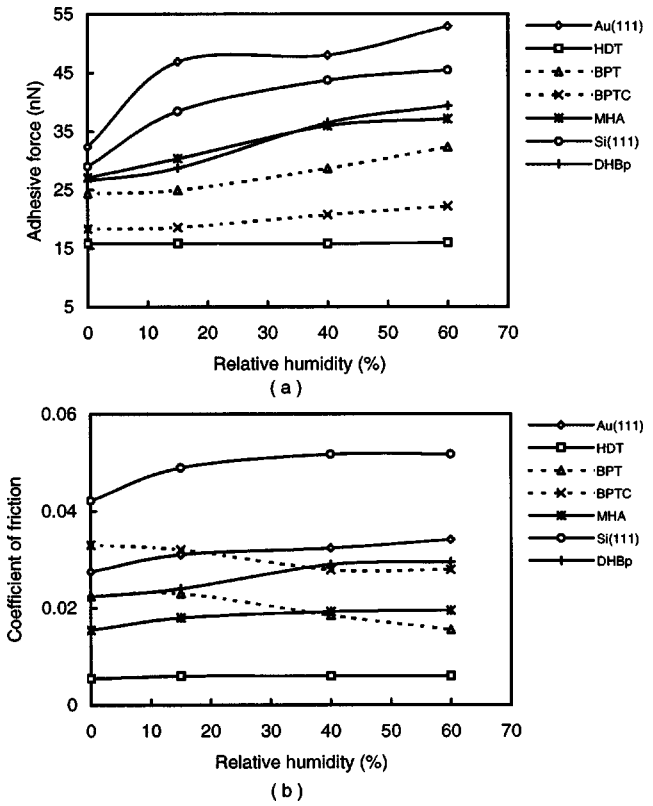

FIG. 12. The influence of relative humidity on the (a) adhesive force and (b) coefficient of friction. All of the points in this figure represent the mean value of six measurements. The uncertainty associated with the average adhesion and friction is within $\pm 8\%$ and $\pm 3\%$, respectively.

TABLE IV. Bond strengths of the chemical bonds in SAMs.

SAMs	Bond	Bond strength[a] (kJ/mol)
Thiol on Au	S-Au	184 (Ref. 37)
Hydroxyl on Si	(Chemical adsorption bond)	242.7 (Ref. 39)
	O-Si	
	(Chemical adsorption bond)	
HDT	H-CH_2	464.8
	H-CH	421.7
	CH_3-t-C_4H_9	425.9 ± 8
	t-C_4H_9-SH	286.2 ± 6.3
MHA	O=CO	532.2 ± 0.4
	H-$OCOC_2H_5$	445.2 ± 8
	HO-$OCH_2C(CH_3)$	193.7 ± 7.9
	$C_6H_5CH_2$-COOH	280
BPT	CH_3-CH_3	376.0 ± 2.1
	$H_2C=CH_2$	733 ± 8
	C_6H_5-SH	361.9 ± 8
DHBp	C_6H_5-H	361.9 ± 8

[a]Most of the data cited are from Ref. 40, except as indicated otherwise. For MHA and DHBp, the bonds that are common as in HDT and DHBp are repeated.

IV. CONCLUSIONS

In this study, five kinds of alkylthiol and biphenyl thiol SAMs with different surface terminals and head groups have been prepared. The adhesion, friction, and wear properties

were investigated by AFM. The friction and wear mechanisms of SAMs were discussed at a molecular level.

SAMs can significantly reduce the adhesive and frictional forces of silicon. The HDT film with a $-CH_3$ terminal exhibits the lowest adhesive force and frictional force, because of its low work of adhesion terminal and its highly compliant long carbon chain. The adhesive force can be influenced by the formation of water capillary. A linear relationship exists between the adhesive force and the work of adhesion of the tested samples. The molecular spring model is presented to describe the friction behavior of SAMs. It is suggested that SAMs exhibit compliance, which allow them to undergo orientation under normal load. The orientation of SAMs reduces the shear stress on the interface; therefore SAMs can serve as lubricants. The molecular spring constant as well as the intermolecular forces can determine the magnitude of the coefficients of friction of SAMs.

DHBp, due to its rigid biphenyl spacer chains, stronger interfacial bonds, and hard substrate, has the highest wear resistance. For all of the SAMs, the wear depth with normal load curves show critical normal loads. Below the critical normal loads, SAMs undergo orientation, while at the critical normal loads SAMs undergo severe wear at the interface due to the weak interface bond strengths. In order to improve the wear resistance, the interfacial bond must be enhanced, and a hard substrate is also preferred.

The influence of relative humidity on adhesive and frictional forces can be mainly understood by comparing their surface terminal polarization properties and work of adhesion. Comparing with Si(111), Au(111), DHBp, and MHA, the tribological properties of BPT and BPTC are less sensitive to changes in humidity, while HDT is not sensitive to humidity changes. At higher humidity, water capillary condensation can either increase friction through increased adhesion in the contact zone or reduce friction through an enhanced water-lubricating effect.

ACKNOWLEDGMENTS

The authors thank Dr. W. Eck, Mr. V. Stadler, and Professor M. Grunze, of University of Heidelberg, Germany for preparing SAM samples, as well as many helpful discussions. The financial support for this research was provided by the National Science Foundation (Contract NO. ECS-9820022). The content of this information does not necessarily reflect the position or policy of the Government and no official endorsement should be inferred.

*Corresponding author. Electronic address: Bhushan.2@osu.edu

[1] B. Bhushan, *Tribology Issues and Opportunities in MEMS* (Kluwer Academic, Dordrecht, Netherlands, 1998).
[2] B. Bhushan, *Handbook of Micro/Nanotribology*, 2nd ed. (CRC, Boca Raton, FL, 1999).
[3] B. Bhushan, J. N. Israelachvili, and U. Landman, Nature (London) **374**, 607 (1995).
[4] B. Bhushan, *Principles and Application of Tribology* (Wiley, New York, 1999).
[5] B. Bhushan, *in Modern Tribology Handbook*, edited by B. Bhushan (CRC, Boca Raton, FL, 2001), pp. 909–929.
[6] A. Ulman, *An Introduction to Ultrathin Organic Films: From Langmuir-Blodgett to Self-Assembly* (Academic, San Diego, CA, 1991).
[7] A. Ulman, Chem. Rev. **96**, 1533 (1996).
[8] Y. Xia and G. M. Whitesides, Angew. Chem. Int. Ed. Engl. **37**, 550 (1998).
[9] R. W. Carpick and M. Salmeron, Chem. Rev. **97**, 1163 (1997).
[10] V. DePalma and N. Tillman, Langmuir **5**, 868 (1989).
[11] E. Ando, Y. Goto, K. Morimoto, K. Ariga, and Y. Okahata, Thin Solid Films **180**, 287 (1989).
[12] J. Ruhe, V. J. Novotny, K. K. Kanazawa, T. Clarke, and G. B. Street, Langmuir **9**, 2383 (1993).
[13] B. Bhushan, A. V. Kulkarni, V. N. Koinkar, M. Boehm, L. Odoni, C. Martelet, and M. Belin, Langmuir **11**, 3189 (1995).
[14] Y. Liu, T. Wu, and D. F. Evans, Langmuir **10**, 2241 (1994).
[15] Y. Liu, D. F. Evans, Q. Sun, and D. W. Grainger, Langmuir **12**, 1235 (1996).
[16] X. Xiao, J. Hu, D. H. Charych, and M. Salmeron, Langmuir **12**, 235 (1996).
[17] A. Lio, D. H. Charych, and M. Salmeron, J. Phys. Chem. B **101**, 3800 (1997).
[18] M. T. McDermott, J. B. D. Green, and M. D. Porter, Langmuir **13**, 2504 (1997).
[19] H. Schonherr and G. J. Vancso, Mater. Sci. Eng., C **8–9**, 243 (1999).
[20] H. I. Kim, T. Koini, T. R. Lee, and S. S. Perry, Langmuir **13**, 7192 (1997).
[21] H. I. Kim, M. Graupe, O. Oloba, T. Koini, S. Imaduddin, T. R. Lee, and S. S. Perry, Langmuir **15**, 3179 (1999).
[22] V. V. Tsukruk, M. P. Everson, L. M. Lander, and W. J. Brittain, Langmuir **12**, 3905 (1996).
[23] S. Lee, Y. S. Shon, T. R. Lee, and S. S. Perry, Thin Solid Films **358**, 152 (2000).
[24] G. Y. Liu, S. Xu, and S. C. Dupeyrat, in *Thin Films* (Academic, San Diego, CA, 1998), pp. 81–110.
[25] W. Geyer, V. Stadler, W. Eck, M. Zharnikov, A. Golzhauser, and M. Grunze, Appl. Phys. Lett. **75**, 2401 (1999).
[26] J. Ruan and B. Bhushan, ASME J. Tribol. **116**, 378 (1994).
[27] H. Liu, B. Bhushan, W. Eck, A. Golzhauser, V. Stadler, and W. Geyer, J. Vac. Sci. Technol. A (to be published).
[28] S. Sundararajan and B. Bhushan, J. Appl. Phys. **88**, 4825 (2000).
[29] Y. F. Miura, M. Takenga, T. Koini, M. Graupe, N. Garg, R. L. Graham, and T. R. Lee, Langmuir **14**, 5821 (1998).
[30] M. Ratajczak-Sitarz, A. Katrusiak, Z. Kaluski, and J. Garbarczyk, Acta Crystallogr., Sect. C: Cryst. Struct. Commun. **43**, 2389 (1987).
[31] J. N. Israelachvili, *Intermolecular and Surface Forces*, 2nd ed. (Academic, London, 1992).
[32] R. J. Good and C. J. van Oss, *Modern Approaches to Wettability—Theory and Applications* (Plenum, New York, 1992).
[33] M. H. V. C. Adao, B. J. V. Saramago, and A. C. Fernandes, J. Colloid Interface Sci. **217**, 94 (1999).
[34] Y. Unno, H. Kawamura, H. Kita, and S. Sekiyama, in Advanced

Ceramics, Structure, and Tribology Applications, Proceedings of the International Symposium (Canadian Institute of Mining, Metallurgy and Petroleum, Montreal, Canada, 1995), pp. 275–284.

[35] J. I. Siepmann and I. R. McDonald, Phys. Rev. Lett. **70**, 453 (1993).

[36] M. Garcia-Parajo, C. Longo, J. Servat, P. Gorostiza, and F. Sanz, Langmuir **13**, 2333 (1997).

[37] A. Lio, C. Morant, D. F. Ogletree, and M. Salmeron, J. Phys. Chem. B **101**, 4767 (1997).

[38] E. Barrena, S. Kopta, D. F. Ogletree, D. H. Charych, and M. Salmeron, Phys. Rev. Lett. **82**, 2880 (1999).

[39] T. Hoshino, C. Yayoi, and K. Inage, J. Phys.: Condens. Matter **59**, 2332 (1999).

[40] D. R. Lide, *CRC Handbook of Chemistry and Physics*, 75th ed. (CRC, Boca Raton, FL, 1994).